Biocidal polymer derived near white light-emitting carbonized polymeric dots for antibacterial and bioimaging applications

Shaifali Sartaliya, Raina Sharma, Anjana Sharma, Vianni Chopra, Neethu K. M, Deepa Ghosh and Govindasamy Jayamurugan*

Institute of Nano Science and Technology, Knowledge City, Sector 81, SAS Nagar, Manauli PO, Mohali, Punjab 140306, India

E-mail: jayamurugan@inst.ac.in

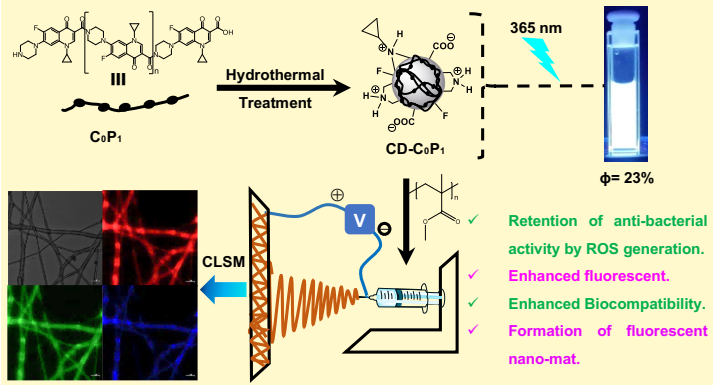

Keywords: Carbonized polymer dots, near white light emission, antibacterial activity, bioimaging, electrospinning, nanofiber mat.

ABSTRACT: A growing antimicrobial crisis has increased demand for antimicrobial materials. It has become increasingly popular to convert polymeric macromolecules into carbonized polymer nanodots (CPDs) in order to achieve highly biocompatible materials with unique properties as a result of the ability to synthesize nanomaterials of the right size and add value to existing stable polymers. This work presents the tuning of polymeric carbon dots (PCDs) for antibacterial application by combining a biocidal polymer with one-pot solvothermal synthesis. PCDs displayed broad-spectrum antibacterial activity *via* various mechanisms, including inhibition of bacterial cell walls, ROS generation, and antibiotic resistance. Further, these biocidal PCDs were observed to show excitation-independent near-white light emission which on the other hand is generally possible due to mixed sizes, doping, and surface effects. As opposed to the parent biocidal polymer, CD added ROS-mediated bactericidal activity, increased cytocompatibility and nanofibers with anti-adhesive effects and potential of imaging bacterial cells.

INTRODUCTION

A revolution in modern medicine based on antibiotics has saved millions of lives since penicillin was discovered.[1] The continual and unpredictable evolution of microorganisms has resulted in the emergence and re-emergence of new infectious diseases, which prevailed a burden in health care infrastructure.[2] Developing new antimicrobial drugs with low toxicity, significant biocompatibility, excellent antimicrobial activity with newer mechanisms of action is urgently needed.[3,4] However, it is also critical to make use of and improve the effectiveness of existing antibiotics.[5] Antimicrobial nanotechnology has emerged as a promising field recently. In which, carbon based nanomaterials such as carbon nanotubes (CNTs), graphene oxide (GO), fullerenes are reported to act as potent antimicrobial agents.[6-8] Lately, carbon dots (CD) have been discovered to be a valuable material due to its outstanding optoelectronic properties and high biocompatibility.[9,10] CDs have also emerged as new antimicrobial agents with novel and complex mode of action which involve ROS generation, cell wall degeneration, photosensitization, electrostatic interaction, and photothermal- and hyperthermia-induced programmed bactericidal activity, etc.[11-14]

While carbonized polymeric dots (CPD) is being extensively studied as new light emitting materials,[15] the CPD formation using polymers provide apparent advantage of the ability to control size while synthesis by tuning the applied 'cracking force' and to retain the surface functionalities compared to the smaller precursor molecules. For instance, Xi and co-workers have synthesized fluorescent CPD materials with different core sizes in one step by hydrothermal treatment of amide abundant polyacrylamide for bioimaging purspose.[16] Tao et al. have also designed room temperature phosphorescence generating PCDs using polyacrylic acid and ethylene diamine *via* single step hydrothermal reaction.[17]

The better biocompatibility, reduced toxicity, economical fabrication, and surface functionalization of CPDs has attracted various groups for establishing CPD's antibacterial profile.[18,19] Recently, Maruthapandi et al. reported the formation of carbon nanocomposites using positively charged conducting polymers polyaniline and polypyrrole for antibacterial property.[20] Jijie et al. have conjugated ampicillin antibiotic to post-synthesized CDs and observed retainment of antibacterial acitivity.[21] Using oligomeric polyethyleneimine as a surface functionalization-passivation agent, Abu Rabe et al. prepared core-shell type CDs with relatively simple chemical compositions which was further used for photodynamic inactivation of multidrug resistant bacteria.[22] However, to the best of our knowledge, CPD of polymeric biocides with the retention or enhanced activity has not been reported.

Recently, we have reported a true polymeric biocide **C_0P_1** having only drug units comprising of broad-spectrum antibiotic ciprofloxacin **1** via self-condensation reaction for antibacterial coating application.[23] In an attempt to synthesize highly biocompatible and fluorescent material with bioimaging application derived from true polymeric biocide, herein, we synthesized the CPD of **C_0P_1**[23] (CPD-**C_0P_1**) and optimized its synthesis for white light (WL) emission property (Scheme 1). Due to its higher molecular weight (973 KDa; DLS size: 1 μm (Figure S6a, SI)), biocidal polymer **C_0P_1** has been chosen as a carbon source, suitable for top-down synthetic approach for controlling the size of carbon nanocomposites that can degenerate cell wall and generate ROS for bacterial cell death.

EXPERIMENTAL SECTION

Synthesis of CPD-C_0P_1: Typically, 10 mg of **C_0P_1** was dissolved in 2 mL of hexamethylphosphoramide (HMPA) and stirred well for 10–15 min to obtain a homogenous solution. Which was further transferred to a 25 mL capacity Teflon-lined hydrothermal reactor and heated in muffle furnace at 200 °C for 24 h. The reactor was opened after cooling to room temperature, to obtain homogeneous and dark brown color solution. The solution was diluted with H_2O (20 mL) and kept in a dialysis bag with MWCO 1000 Da against H_2O (250 mL × 2) for 24 h to remove the HMPA and the inner part of dialysis bag was lyophilized and recovered as brownish powder (4.21 mg) **CPD-C_0P_1**.

RESULTS AND DISCUSSION

Synthesis and characterization

Polymeric biocide (**C_0P_1**) derived carbonized polymeric dots (**CPD-C_0P_1**) were synthesized *via* a solvothermal approach, monitored by fluorescence emission of reaction mixture.

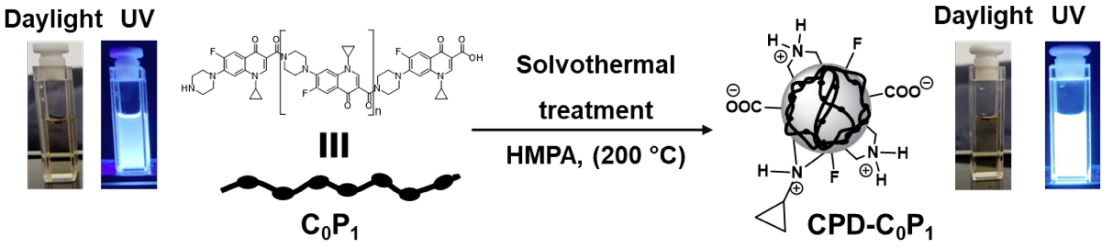

Scheme 1. Solvothermal mediated conversion of biocidal polymer to carbonized polymeric dot **CPD-C_0P_1.**

For the optimization of solvothermal reaction conditions (Table 1), the polymer **C_0P_1**[23] was thermally treated along with different high boiling solvents (DMSO, EtOH, and HMPA) at varying temperature (150–220 °C) and time period (24–72 h). After completion of the time, the reaction mixtures were scanned for the presence of emission (Table 1, Figure S1) and size of the CPD through DLS analysis. The results revealed that DMSO and EtOH did not provide emissive CPD due to larger particles and precipitation, respectively (entries 1–9, Table 1). Interestingly, hexamethylphosphoramide (HMPA) has provided relatively smaller sized CPDs with emissive nature (entries 10–14). A **CPD-C_0P_1** with a size of 120–270 nm (size by DLS analysis of reaction mixture) was obtained under entry 11 (200 °C for 24 h), which was selected as an optimized condition due to its near WL color and higher emission intensity. The fluorescence intensity was observed to be affected by the reaction temperature and time period even with HMPA. **CPD-C_0P_1** obtained under entry 11 condition was taken forward for further characterization and antibacterial studies.

Table 1. Optimization table for the generation of fluorescent **CPD-C_0P_1** from **C_0P_1**.[a]

Entry	Reaction mixture	Solvent	Temperature (°C)	Time (h)	Emission[b]	DLS Particle size (nm)
1.	**CPD-C_0P_1**	DMSO	180	24	No	500-1000
2.	**CPD-C_0P_1**	DMSO	200	24	No	500-1000
3.	**CPD-C_0P_1**	DMSO	220	24	No	450-1350
4.	**CPD-C_0P_1**	DMSO	200	48	No	600-1000
5.	**CPD-C_0P_1**	DMSO	200	72	No	550-1120
6.	**CPD-C_0P_1**	DMSO	220	48	No	520-1830
7.	**CPD-C_0P_1**	EtOH	150	24	No	ppt[c]
8.	**CPD-C_0P_1**	EtOH	150	48	No	ppt[c]
9.	**CPD-C_0P_1**	EtOH	180	24	No	ppt[c]
10.	**CPD-C_0P_1**	HMPA	180	24	360–570 nm λ_{max} = 436 nm Blue	426–860
11.	**CPD-C_0P_1**	HMPA	200	24	380–754 nm λ_{max} = 500 nm White-light	120–270
12.	**CPD-C_0P_1**	HMPA	220	24	-	340–672
13.	**CPD-C_0P_1**	HMPA	200	48	370–650 nm λ_{max} = 465 nm green	350–690

14.	**CPD-C_0P_1**	HMPA	200	72	375–560 nm λ_{max} = 478 nm green	260–760

[a]Concentration (0.5 mg/mL) of reaction mixture was kept constant for all reactions, [b]excitation wavelength used was 365 nm, [c]precipitation was observed.

The **CPD-C_0P_1** obtained from biocidal polymer of ciprofloxacin **C_0P_1** has been characterized by a series of methods to analyze the structure and morphology (Figure 1). To figure out the composition and functionality present in the **CPD-C_0P_1**, a comparative ATR-FT-IR analysis of compounds **C_0P_1**, and **CPD-C_0P_1** were carried out (Figure 1a). The characteristic peaks of O–H, N–H, C=O (amide), and C=O (carboxylate) were observed at 3412, 3244, 1630, and 1467 cm^{-1}, respectively indicating the fragmentation of ciprofloxacin unit in **C_0P_1**, thus generating both 3° and 2° amines and carboxylic acid which are in zwitterionic form. The peaks at 1486 and 1392 cm^{-1} indicate the formation of graphitic carbons (C=C).[24] Interestingly, the peak intensity significantly reduced at 1260 cm^{-1}, whereas the new peak 1060 cm^{-1} accredited to the presence of covalent C–F in residual polymer and semi-ionic C–F bond.[25] The peaks at 972 and 737 cm^{-1} indicate the C–C and C–H (bending), respectively.

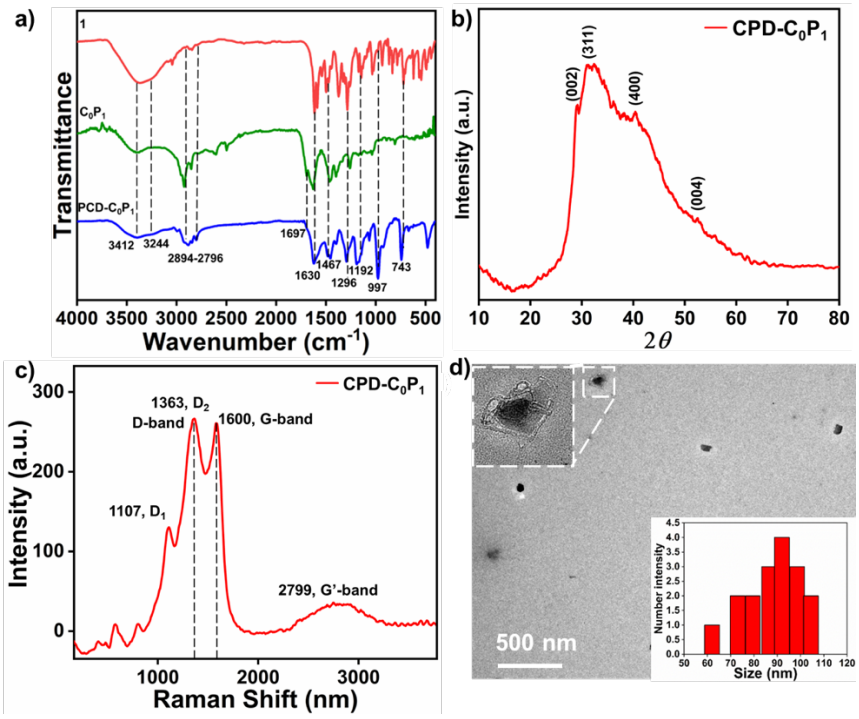

Figure 1 Characterization data, a) FT-IR of 1, **C_0P_1**, **CPD-C_0P_1**, b) P-XRD, c) Raman, b) TEM imaging of **CPD-C_0P_1** (inset: particle size distribution graph).

P-XRD spectrum of **CPD-C_0P_1** shows broad peaks with 002, 311, 400, and 004 plane peaks, where 002 corresponds to graphitic carbon in CD (Figure 1b). These peaks suggest that **CPD-C_0P_1** has an amorphous nature with a certain degree of crystallinity.[26] Additionally,

CPD-C_0P_1's Raman spectrum showed characteristic G- and D-bands, indicating the presence of both graphitic and amorphous carbon in CPD (Figure1c). **CPD-C_0P_1** was examined by TEM for the size of the CPD particles (70–100 nm) and defects on the surface, suggesting the presence of polymers on the surface (Figure 1d), while HR-TEM confirmed the crystallinity in **CPD-C_0P_1** (Figure S3, SI). The DLS analysis further corroborated the size of **CPD-C_0P_1** as ~70–120 nm (Figure S6b,c). Although the size of **CPD-C_0P_1** in the reaction mixture (size mentioned in table 1) and the separated solution was found to be different due to the presence of multispecies (carbon nanotube, polymer etc.) in the reaction mixture after carbonization (Figure S4).Further, the elemental composition was detected using TEM equipped with energy dispersive X-ray (EDX) spectrum for the elements carbon (C, 78%), nitrogen (N, 13%), oxygen (O, 9.3%), and fluorine (F, 0.23%) (Figure S5, Table S1, SI).

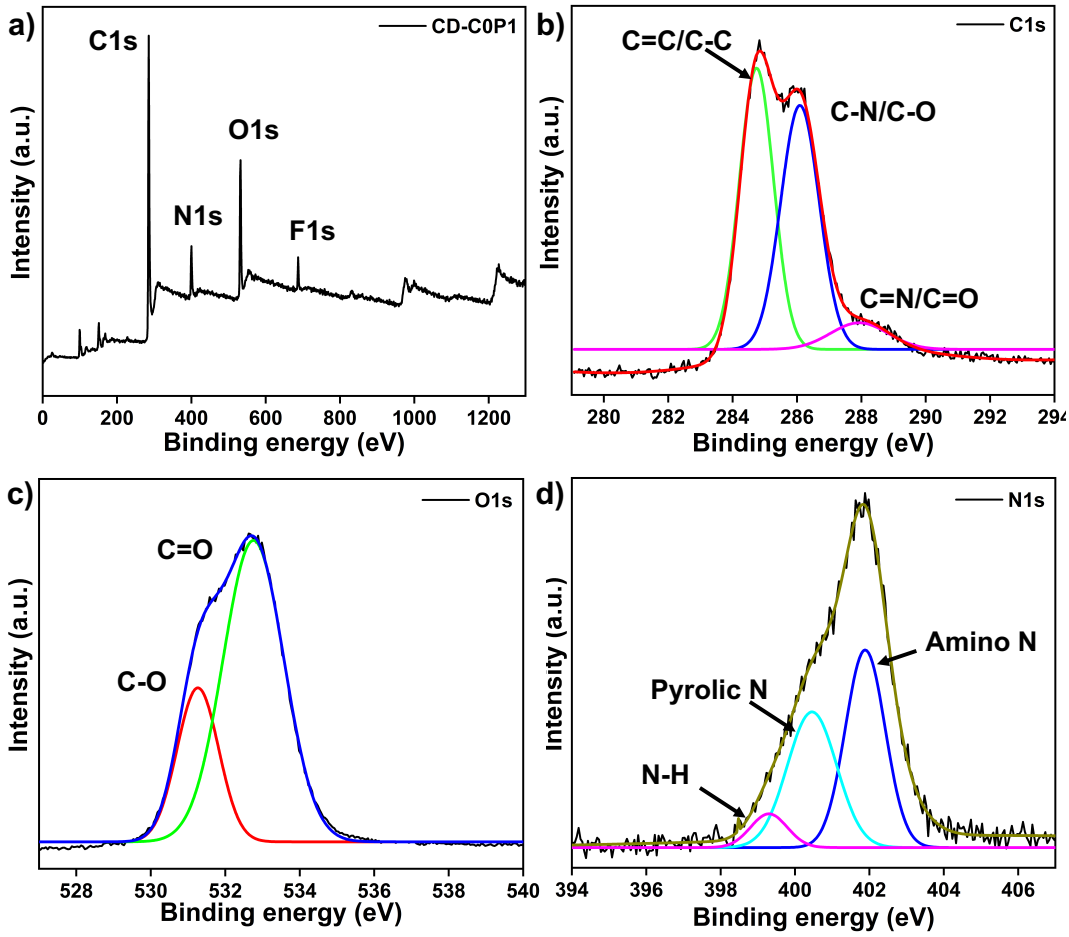

Figure 2. XPS survey of **CPD-C_0P_1** a) broad XPS scan, and the individual high-resolution spectra of b) C 1s, c) O 1s, d) N 1s.

In corroboration with EDX-spectrum, XPS data also indicate the presence of C 1s, N 1s, O 1s and F 1s elements present in CPD (Figure 2). In deconvoluted data for the C 1s, the binding energies for C=C/C–C at 284.71 eV, C–N/C–O at 286.14 eV, and C=N/C=O at 288.02

eV suggest the presence of sp^2 hybridized carbon, while the peaks at 286.14 and 288.02 eV indicate the presence of retentive polymer at the surface of **CPD-C_0P_1** (Figure 2b, SI).[27,28] Similarly, individual curve fittings showed the binding energies for C–O and C=O at 531.22 and 532.77 eV, respectively, indicating the presence of carboxylate functional groups (Figure 2c, SI).[29] A curve fitting for N 1s revealed that amino-, amido-, and positively-charged-*N* have binding energies at 399.2, 400.4, and 401.8 eV, respectively, ascribed to the polymeric structure of **C_0P_1** and the surface functional group present on its surface (Figure 2d, SI).[30,31] A full scan spectrum for **CPD-C_0P_1** (Figure 2a) shows an increase in F1's peak intensity, following **C_0P_1**, indicating traces of fluorine (Figure S7). Further, individually fitted F1s data also revealed semi-ionic C–F bond formation in **CPD-C_0P_1** which was found absent in **C_0P_1** F1s XPS plot (Figure S8).[32]

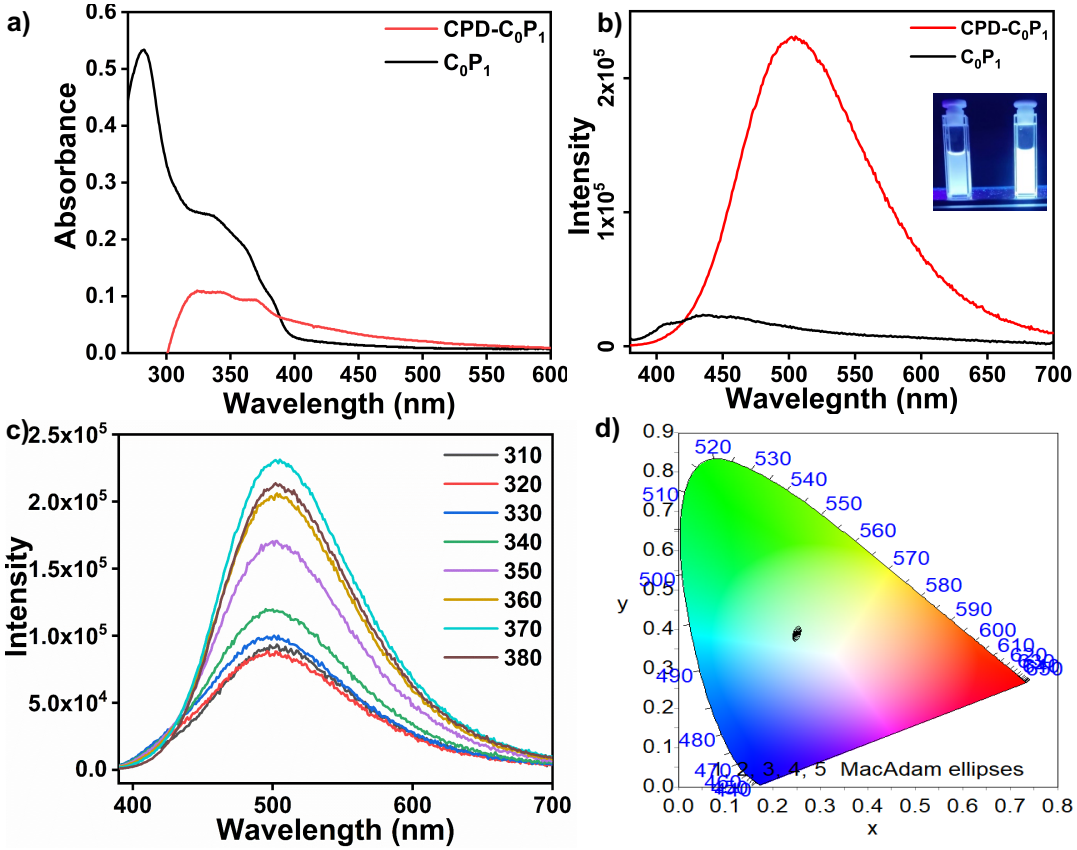

Figure. 3 a) The UV–vis and b) fluorescence (λex=370 nm) spectra of **C_0P_1** and **CPD-C_0P_1** (Inset: solutions under UV lamp), c) fluorescence spectra at different excitation wavelengths for **CPD-C_0P_1**. Concentration 50 µg/mL in DMF.

In order to illustrate the unique emissive nature of CPD, the photophysical properties of **CPD-C_0P_1** were compared with **C_0P_1**. All the spectra were recorded in DMF (50 µg/mL). The UV−vis spectrum of precursor polymer **C_0P_1** has shown absorption at 320–400 nm, while the **CPD-C_0P_1** exhibited broad absorption 320–500 nm (Figure 3a). The broad absorption in

the visible region is due to CPD while the two peaks observed at 345 and 368 nm correspond to π–π* and n–π* transitions. The peak at 281 nm has disappeared for **CPD-C_0P_1** possibly due to the carbonization of polymeric structure. The fluorescence spectra of **CPD-C_0P_1** showed a very weak emission (400–500 nm), whereas the **CPD-C_0P_1** shows a strong and broad emission peak (400–700 nm), owing to the CPD (Figure 3b). Interestingly, the emission was found to show near WL with excitation independent (310–380 nm) emission unlike typical CDs (Figure 3c). The near WL emission was illustrated by the CIE chromaticity diagram with CIE coordinates of 0.25 and 0.38 (Figure 3d). Lifetime measurement was performed for the emission of **CPD-C_0P_1** using time-correlated single photon counting method for further analysis of steady state fluorescence emission. The decay kinetics was successfully fitted to the sum of three exponential components with different time decay of τ_1, τ_2, and τ_3 representing 2.12, 7.49 and 0.26 ns, respectively (Figure S9, Table S2, SI). The quantum yield estimation revealed a moderate value of 23% against quinine sulfate as the reference (Section D2, SI).

Antibacterial activity

The antibacterial activity of **CPD-C_0P_1** was evaluated against Staphylococcus aureus (S. aureus) and Escherichia coli (E. coli) (for experimental details, see Section E, SI) with minimum inhibitory concentration (MIC_{90}) of 25 and 12 μg/mL, respectively (Figure 4a). A time dependent bacterial growth inhibition study was performed by taking the corresponding MIC of **CPD-C_0P_1** and further monitored by optical density (OD600) values measured for cultured bacteria at different times (Figure 4b). While, S. aureus and E. coli in the control group increased significantly at the 4^{th} and 8^{th} h, respectively, and reached a peak at the 16^{th} h for both cases. In contrast, the growth rate of both types of bacteria co-cultured with **CPD-C_0P_1** showed no apparent OD600 increase. This suggests that the **CPD-C_0P_1** shows biocidal activity against both gram-positive and -negative bacteria. For further confirmation, the standard colony counting method was performed to determine the survival of bacteria treated with **CPD-C_0P_1** for 24 h (Figure 4c). The results indicated an apparent decline in bacterial growth with an increasing dose of **CPD-C_0P_1**. At the MIC values complete bacterial growth inhibition was found.

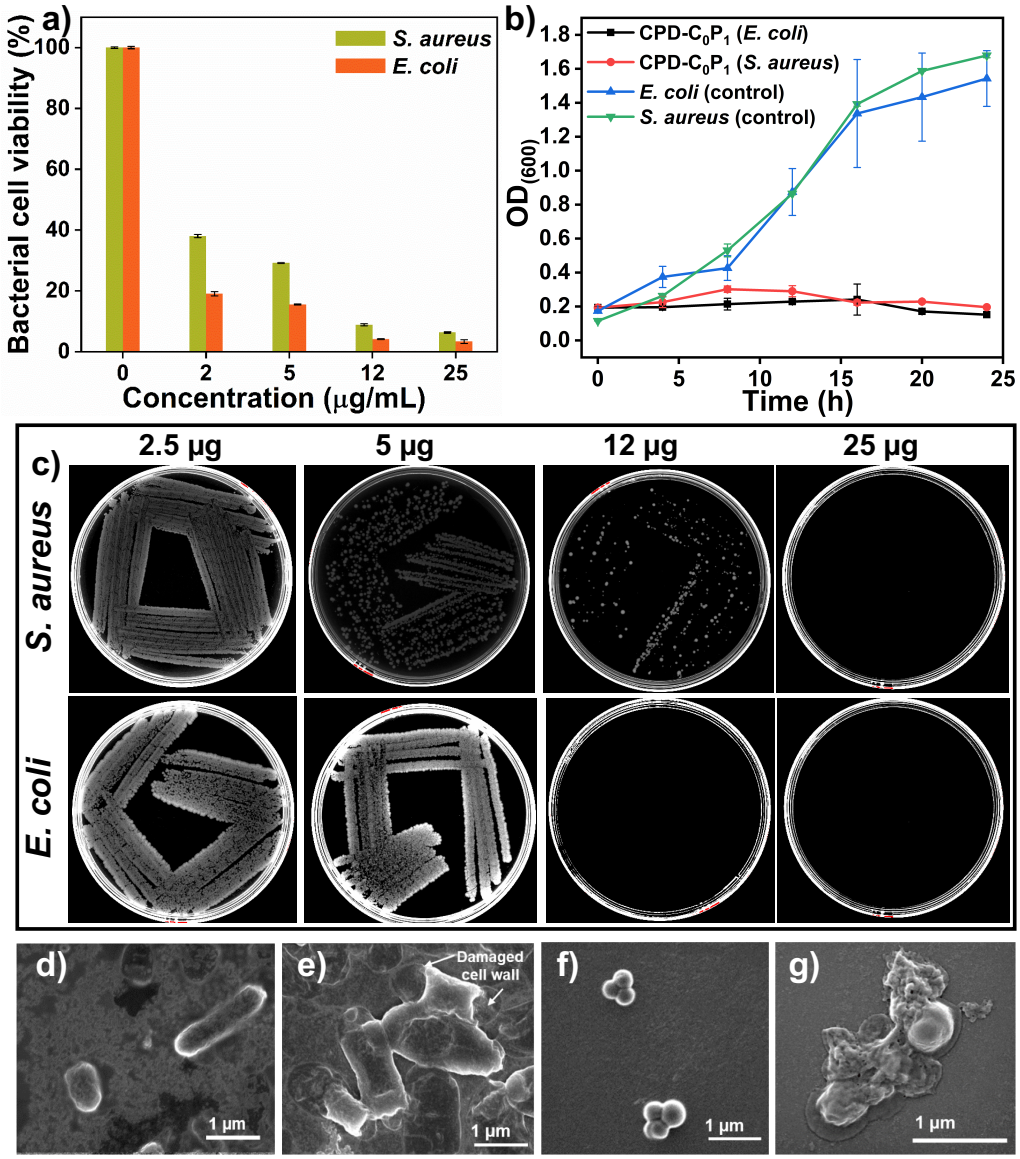

Figure 4 a) Bacterial cell viability (%) of E. coli and S. aureus evaluated after treatment with different concentrations of **CPD-C$_0$P$_1$** after 24 h. b) Time dependent antibacterial activity of **CPD-C$_0$P$_1$** at MIC against E. coli and S. aureus. c) Photographs of E. coli and S. aureus after treating with different concentrations of **CPD-C$_0$P$_1$** for 24 h. FE-SEM imaging of d) E. coli (control), e) after **CPD-C$_0$P$_1$** treatment, f) S. aureus (control), g) after **CPD-C$_0$P$_1$** treatment.

In order to evaluate the cellular damage caused by **CPD-C$_0$P$_1$**, FE-SEM analysis of the bacteria treated with **CPD-C$_0$P$_1$** was performed. This indicated that the bacteria had been killed by ruptured cell walls (Figure 4d-g). Additionally, the **CPD-C$_0$P$_1$** was also observed to adhere specifically to the cell wall of bacteria, governed by surface adherence phenomena and initial electrostatic interactions (Figure S10 SI).[33,14] Further, intrinsic ROS generation was observed in bacterial culture (both E. coli and S. aureus) in the presence of **CPD-C$_0$P$_1$**, even in darkness,

which is a rare occurrence, as determined by ROS determination study using DCFH-DA (for details, see Section F2, SI). Thus, it is possible that intrinsic ROS generation and bacterial cell wall damage contribute significantly to **CPD-C_0P_1**'s biocidal activity.

Cytocompatibility

Cytocompatibility assay was conducted on mouse fibroblast cells and data are provided in Figure 5 (Section E2, SI). Our previous study showed that the precursor biocidal polymer **C_0P_1** has higher cytocompatibility than ciprofloxacin **1** at a concentration of 1 μg/mL.[23] As up-to 90% of cells are unaffected at 500 μg/mL, the **CPD-C_0P_1** shows even greater biocompatibility. Intriguingly, the **CPD-C_0P_1** was found to be highly biocompatible with 10 and 20 times higher concentration against bioactive concentration of S. aureus and E. coli, respectively. Thus, carbonized polymeric dots, as originally hypothesized, could enhance biocompatibility of biocidal polymers.

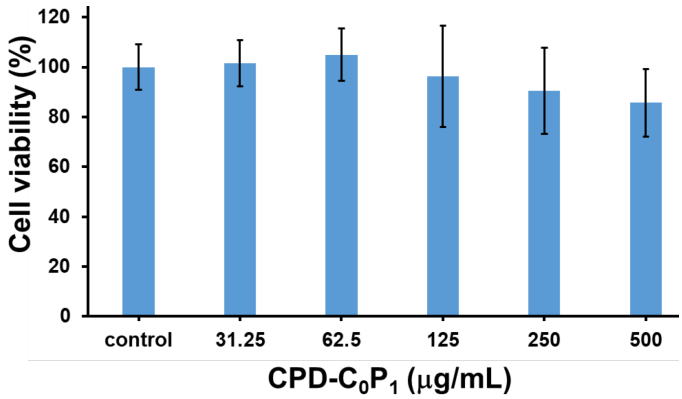

Figure. 5. Cytocompatibility assay of **CPD-C_0P_1** at different concentrations on mouse fibroblast cells.

To demonstrate the practical applications and to fabricate the antimicrobial nanofibers (NF) mat with bio-imaging (RGB colors) capability, the **CPD-C_0P_1** was combined with polymethylmethacrylate (PMMA) matrix and electrospun to obtain nanofibers (for details, see Section G, SI). The NF were prepared by a DMF solution (with optimized concentration of 100 mg in 1 mL) containing PMMA/ **CPD-C_0P_1** (93:7 w/w) as well as only PMMA as control. NF containing PMMA blue fluoresced minimally under confocal microscopy (Figure 6a), whereas, NF containing **CPD-C_0P_1** fluoresced red, green, or blue based on the excitation filter used (TRITC, FITC, and DAPI)[34] and emerged as near WL emitting NF (Figure 6b). The morphology and size of both NFs were characterized by SEM and AFM analysis (Figure S12). Nanofibers with smooth surfaces with a height and width of ~200-400 and ~300-500 nm, respectively have been found for both PMMA and PMMA/**CPD-C_0P_1**. These results imply that the presence of **CPD-C_0P_1** in PMMA did not affect the nanofiber formation significantly. The

PMMA/**CPD-C_0P_1** NFs were further characterized by FT-IR spectroscopy, which revealed the presence of H-bonding interaction between PMMA and **CPD-C_0P_1** (Figure S2).

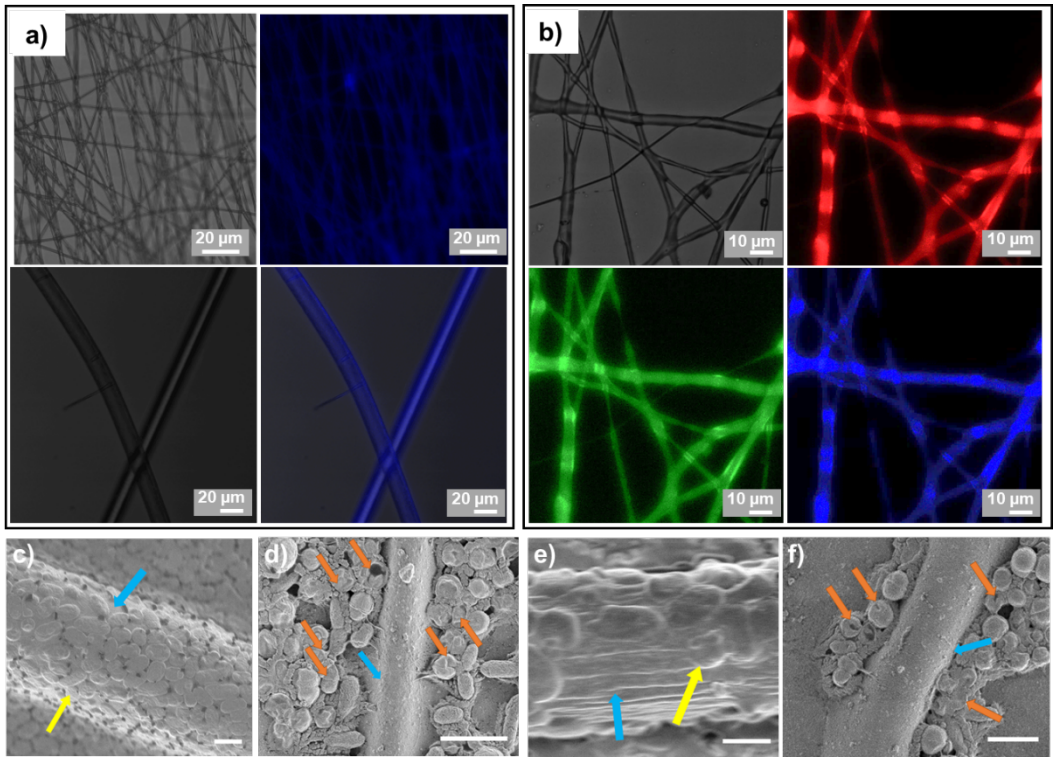

Figure 6 Confocal microscopy images of electro spun nanofibers of a) PMMA, b) PMMA/ **CPD-C_0P_1** 93:7 wt ratio. FE-SEM imaging of (c) E. coli with PMMA NF, (d) E. coli with PMMA/ **CPD-C_0P_1** NF, (e) S. aureus with PMMA NF, and (f) S. aureus with PMMA/ **CPD-C_0P_1** NF.

The antibacterial activity of PMMA/**CPD-C_0P_1** was determined as bacterial growth inhibition measured by visual turbidity readout and release of **CPD-C_0P_1** from the NF (Figure S13–S16, SI). For the release study, the fibers were kept for continuous stirring for 24 h in PBS buffer under dark condition and the fragments of the fibers were collected concerning time (0, 6, 12, and 24 h) and observed for fluorescence intensity by using confocal laser scanning microscopy (CLSM), as the fluorescence in the fibers indicates the presence of **CPD-C_0P_1**. The fluorescence intensity of the fibers reduced gradually with time (Figure S16a,c). Further, the zoomed image of fibers collected at 12 h interval revealed the porosity in fibers which may be due to the release of preblended **CPD-C_0P_1** (Figure S16b). Also, FE-SEM study of fibers at 0 and 12 h revealed the change in morphology after the release of **CPD-C_0P_1** from the fibers (Figure S15).

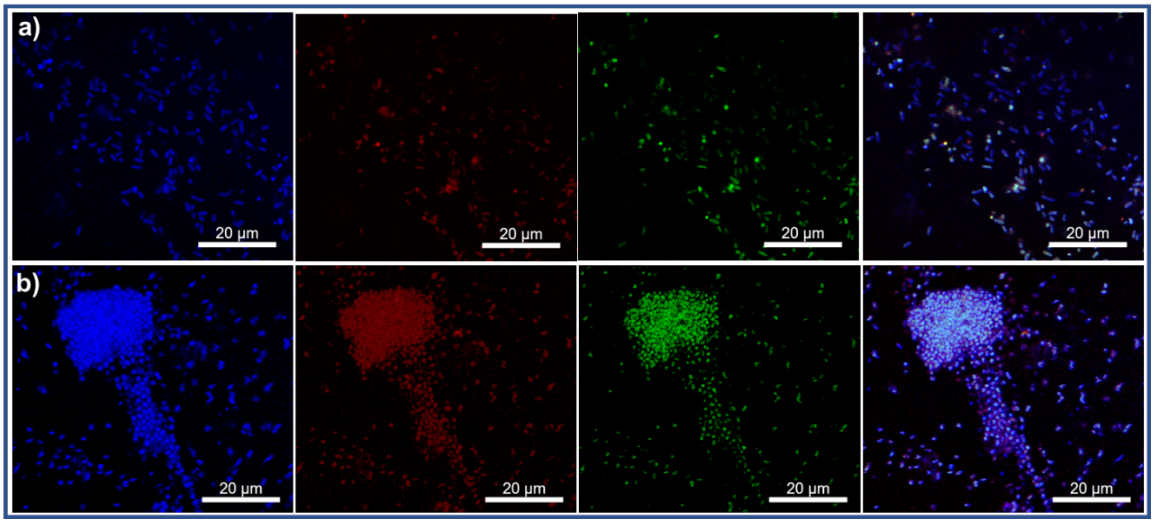

Figure 7. CLSM images of PMMA/**CPD-C_0P_1** treated g) E. coli and h) S. aureus after 6 h.

Further, in both S. aureus and E. coli, the NFs with **CPD-C_0P_1** showed higher biocidal activity by inhibiting bacterial growth at different time points (0, 6, 12 h) with regards to OD(600) (Figure S13). However, a rapid growth of bacteria was observed with bare PMMA fibers. Moreover, ~90% of bacterial colonies were inhibited within 12 h by the aliquots of PMMA/ **CPD-C_0P_1** streaked on solidified agar plates (Figure S14), suggesting that **CPD-C_0P_1** is constantly released from PMMA/ **CPD-C_0P_1**. After 12 h of incubation in bacterial medium, the PMMA and PMMA/**CPD-C_0P_1** NFs were visualized by FE-SEM for fiber-bacterial interactions. The bare PMMA NF is observed to soak through by E. coli and S. aureus (Figure 6c&e). In contrast, no bacteria adhered to PMMA/**CPD-C_0P_1** because of its antiadhesive properties (Figure 6d&f). In addition, all the bacteria present around PMMA/**CPD-C_0P_1** NFs displayed damaged cell walls. It appears that the presence of **CPD-C_0P_1** in inert PMMA NF may confer antibacterial activity to PMMA/**CPD-C_0P_1** NF. Using CLSM, the E. coli and S. aureus treated with PMMA/**CPD-C_0P_1** NFs were found to be fully taken up by the bacteria, indicating that **CPD-C_0P_1** may be effective as fluorescent imaging agent for bacterial cells (Figure 7a and b).

Conclusion. In summary, by utilizing the top-down approach, we optimized the condition to obtain excitation independent near WL emitting carbon dots **CPD-C_0P_1** with 23% quantum yield. The resulting antimicrobial **CPD-C_0P_1** not only retained the antibacterial effect but also exhibited improved biocompatibility. Further, we demonstrated a successful fabrication of nanofibers using PMMA as matrix to provide RGB emissive antimicrobial NF mat. Mechanistic studies revealed that **CPD-C_0P_1** was found to be intrinsically generating the ROS and resulting in programmed bacterial cell death. This work has the potential to significantly

impact the development of better and biocompatible antimicrobial materials, despite the fact that carbon nanomaterials are emerging as promising bioactive materials

Conflicts of Interest

The authors declare no conflicts.

Acknowledgements

This work was supported by the SERB, Department of Science and Technology (DST), grant nos. SB/S2/RJN-047/2015 and CRG/2022/007139. GJ thanks DST-SERB for Ramanujan Fellowship.

References

1. Cunha, B. R. da; Fonseca, L. P.; Calado, C. R. C. Antibiotic Discovery: Where Have We Come from, Where Do We Go?. *Antibiotics* **2019**, *8*, 45.
2. Morens, D.; Folkers, G.; Fauci, A. The challenge of emerging and re-emerging infectious diseases. *Nature* **2004**, *430*, 242.
3. Toprak, E; Veres, A.; Michel, J. B.; Chait, R.; Hartl, D. L.; Kishony, R. Evolutionary paths to antibiotic resistance under dynamically sustained drug selection. *Nat. Genet.* **2012**, *44*, 101.
4. Laxminarayan, R.; Matsoso, P.; Pant, S.; Brower, C.; Røttingen, J. A.; Klugman K.; Davies, S. Access to effective antimicrobials: a worldwide challenge. *Lancet* **2016**, *387*, 168.
5. León-Buitimea, A.; Garza-cárdenas, C. R.; Garza-cervantes, J. A.; Lerma-Escalera, J. A.; Morones-Ramírez, J. R. The Demand for New Antibiotics: Antimicrobial Peptides, Nanoparticles, and Combinatorial Therapies as Future Strategies in Antibacterial Agent Design. *Front. Microbiol.* **2020**, *11*, 1.
6. Al-Jumaili, A.; Alancherry, S.; Bazaka, K.; Jacob, M.V. Review on the Antimicrobial Properties of Carbon Nanostructures. *Materials* **2017**, *10*, 1066.
7. Mocan, T.; Matea, C.T.; Pop, T.; Mosteanu, O.; Buzoianu, A.D.; Suciu, S.; Puia, C.; Zdrehus, C.; Iancu, C.; Mocan, L. Carbon nanotubes as anti-bacterial agents. *Cell. Mol. Life Sci.* **2017**, *74*, 3467.
8. Liu, H.; Zhang, L.; Yan, M.; Yu, J. Carbon nanostructures in biology and medicine. *J. Mater. Chem. B.* **2017**, *5*, 6437.
9. Lim, S. Y.; Shen, W.; Gao, Z. Carbon quantum dots and their applications. *Chem. Soc. Rev.*, **2015**, *44*, 362.

10. Xu, J. W.; Yao K.; Xu, Z. K. Nanomaterials with a photothermal effect for antibacterial activities: an overview. *Nanoscale* **2019**, *11*, 8680.
11. Du, J.; Xu, N.; Fan, J.; Sun, W.; Peng, X. Carbon Dots for In Vivo Bioimaging and Theranostics. *Small* **2019**, *15*, 1805087.
12. Su, W.; Wu, H.; Xu, H.; Zhang, Y.; Li, Y.; Li, X.; Fan, L. Carbon dots: a booming material for biomedical applications. *Mater. Chem. Front.* **2020**, *4*, 821.
13. Varghese, M.; Balachandran, M. Antibacterial efficiency of carbon dots against Gram-positive and Gram-negative bacteria: A review. *J. Environ. Chem. Eng*. **2021**, *9*, 106821.
14. Liang, J.; Li, W.; Chen, J.; Huang, X.; Liu, Y.; Zhang, X.; Shu, W.; Lei, B.; Zhang, H. Antibacterial Activity and Synergetic Mechanism of Carbon Dots against Gram-Positive and -Negative Bacteria. *ACS Appl. Bio Mater*. **2021**, *4*, 6937.
15. Tao, S.; Feng, T.; Zheng, C.; Zhu, S.; Yang, B. Carbonized Polymer Dots: A Brand New Perspective to Recognize Luminescent Carbon-Based Nanomaterials. *J. Phys. Chem. Lett.* **2019**, *10*, 5182.
16. Gu, J.; Wang, W.; Zhang, Q.; Meng, Z.; Jia, X.; Xi, K. Synthesis of fluorescent carbon nanoparticles from polyacrylamide for fast cellular endocytosis. *RSC Adv.* **2013**, *3*, 15589.
17. Tao, S.; Lu, S.; Geng, Y.; Zhu, S.; Redfern, S. A. T.; Song, Y.; Feng, T.; Xu, W.; Yang, B. Design of Metal-Free Polymer Carbon Dots: A New Class of Room-Temperature Phosphorescent Materials. *Angew. Chem. Int. Ed.* **2018**, *57*, 2393.
18. Zhu, S.; Song, Y.; Zhao, X.; Shao, J.; Zhang, J.; Yang, B. The photoluminescence mechanism in carbon dots (graphene quantum dots, carbon nanodots, and polymer dots): Current state and future perspective. *Nano Res.* **2015**, *8*, 355.
19. Mansuriya, B.D.; Altintas, Z. Carbon Dots: Classification, Properties, Synthesis, Characterization, and Applications in Health Care—An Updated Review (2018–2021). *Nanomaterials* **2021**, *11*, 2525.
20. Maruthapandi, M.; Saravanan, A.; Gupta, A.; Luong, J. H. T. Gedanken, A. Antimicrobial Activities of Conducting Polymers and Their Composites. *Macromol*. **2022**, *2*, 78.
21. Jijie, R.; Barras, A.; Bouckaert, J.; Dumitrascu, N.; Szunerits, S.; Boukherroub, R. Enhanced antibacterial activity of carbon dots functionalized with ampicillin combined with visible light triggered photodynamic effects. *Colloids Sur. B: Biointerfaces* **2018**, *170*, 347.
22. Abu Rabe, D. I.; Mohammed, O. O.; Dong, X.; Patel, A. K.; Overton, C. M.; Tang, Y.; Kathariou, S.; Sun, Y. P.; Yang, L.; Carbon dots for highly effective photodynamic inactivation of multidrug-resistant bacteria. *Mater. Adv.* **2020**, *1*, 321.

23. Sartaliya, S.; Gowri, V.; Chopra, V.; Roy, H. S.; Ghosh D.; Jayamurugan, G. Unraveling the Effect of Nondrug Spacers on a True Drug-Polymer and a Comparative Study of Their Antimicrobial Activity. *ACS Appl. Polym. Mater.* **2022**, *4*, 3952.
24. Tan, J.; Zou, R.; Zhang, J.; Li, W.; Zhang, L.; Yue, D. Large-scale synthesis of N-doped carbon quantum dots and their phosphorescence properties in a polyurethane matrix. *Nanoscale* **2016**, *8*, 4742.
25. Kang, W.; Li, S. Preparation of fluorinated graphene to study its gas sensitivity. *RSC Adv.* **2018**, *8*, 23459.
26. Li, J. H. T.; Kang, Z. H.; Liu, Y.; Lee, S.-T. Carbon nanodots: synthesis, properties and applications. *J. Mater. Chem.* **2012**, *22*, 24230.
27. Niu, Q.; Gao, K.; Lin, Z.; Wu, W. Amine-capped carbon dots as a nanosensor for sensitive and selective detection of picric acid in aqueous solution via electrostatic interaction. *Anal. Methods* **2013**, *5*, 6228.
28. Chen. W.; Li, D.; Tian, L.; Xiang, W.; Wang, T.; Hu, W.; Dai, Z. Synthesis of graphene quantum dots from natural polymer starch for cell imaging. *Green Chem.* **2018**, *20*, 4438.
29. Al-Gaashani, R.; Najjar, A.; Zakaria, Y.; Mansour S.; Atieh, M. A. XPS and structural studies of high quality graphene oxide and reduced graphene oxide prepared by different chemical oxidation methods. *Ceram. Int*. **2019**, *45*, 14439.
30. Yuan, S.; Xiong, G.; He, F.; Jiang, W.; Liang, B.; Choong, C. Multifunctional REDV-conjugated zwitterionic polycarboxybetaine–polycaprolactone hybrid surfaces for enhanced antibacterial activity, anti-thrombogenicity and endothelial cell proliferation. *J. Mater. Chem. B*. **2015**, *3*, 8088.
31. Bleu, Y.; Barnier, V.; Christien, F.; Bourquard, F.; Loir, A.; Garrelie, F.; Donnet, C. Dynamics of carbon diffusion and segregation through nickel catalyst, investigated by in-situ XPS, during the growth of nitrogen-doped graphene. *Carbon* **2019**, *155*, 410.
32. Lee, J. W.; Jeong, S. P.; You N.-H.; Moon, S.-Y. Tunable Synthesis of Predominant Semi-Ionic and Covalent Fluorine Bonding States on a Graphene Surface. *Nanomaterials* **2021**, *11*, 942.
33. Bing, W.; Sun, H.; Yan, Z.; Ren J.; Qu, X. Programmed Bacteria Death Induced by Carbon Dots with Different Surface Charge. *Small* **2016**, *12*, 4713.
34. Dar, A. H.; Gowri, V.; Mishra, R. K.; Khan, R.; Jayamurugan, G. Nanotechnology-Assisted, Single-Chromophore-Based White-Light-Emitting Organic Materials with Bioimaging Properties. *Langmuir* **2022**, *38*, 430.

Biocidal polymer derived near white light-emitting carbonized polymeric dots for antibacterial and bioimaging applications